PNAS
www.pnas.org

Supplementary Information for

Defined core-shell particles as the key to complex interfacial self-assembly

Johannes Menath[a], Jack Eatson[b], Robert Brilmayer[c], Annette Andrieu-Brunsen[c], D. Martin A. Buzza [b] and Nicolas Vogel[a]

[a] Institute of Particle Technology, Friedrich-Alexander University Erlangen-Nürnberg, Cauerstrasse 4, 91058 Erlangen, Germany
[b] G W Gray Centre for Advanced Materials, Department of Physics and Mathematics, University of Hull, Hull HU6 7RX, United Kingdom
[c] Macromolecular Chemistry - Smart Membranes, Technical University of Darmstadt, Alarich-Weiss-Str. 8, 64287 Darmstadt, Germany

Nicolas Vogel

Email: nicolas.vogel@fau.de

This PDF file includes:

Other supplementary materials for this manuscript include the following:

Supplementary Discussion

Simple model for the interaction potential between crosslinked and uncrosslinked shells

We first consider the case of crosslinked shells where the shell protrudes significantly into the water subphase (see Figure 1a top).(1–3) To simplify our discussion, we approximate the quasi three-dimensional shape of the soft shell as two wide-based cones (base radius $r_1/2$) with their bases stuck together and their axis of symmetry perpendicular to the liquid interface (Figure S13a,b and Figure 1a top). From simple geometry, the angle ψ is given by $\sin\psi = r_0/r_1$ while the height of the shell as a function of the radial distance ρ is $h(\rho) = \tan\psi\left(\frac{r_1}{2} - \rho\right)$. We can approximate the interaction potential between two core-shell particles with separation r as (4)

$$U(r) \approx P_{corona} V_{intersect}(r) \qquad (1)$$

where P_{corona} is the pressure exerted by the soft shell for typical microgel concentrations found in the interacting soft shells and $V_{intersect}(r)$ is the intersection volume between the two soft shells at separation r (see Figure S13a,b). The volume of the volume element corresponding the partial anulus shown in Figure S13b is given by

$$dV = 8\rho\theta h(\rho) d\rho \qquad (2)$$

where $\theta = \cos^{-1}(r/2\rho)$ so that the intersection volume is given by

$$V_{intersect}(r) = 2\tan\psi \int_{r/2}^{r_1/2} \cos^{-1}\left(\frac{r}{2\rho}\right)\rho\left(\frac{r_1}{2} - \rho\right) d\rho. \qquad (3)$$

Inserting Eq.(3) into Eq.(1) and defining U_0 as the interaction potential at core contact we finally have

$$U(r) = U_0 \frac{V_{intersect}(r)}{V_{intersect}(r_0)} \qquad (4)$$

which is plotted in Figure 1b for the case of $r_1/r_0 = 4$ (red curve).

We next consider the case of uncrosslinked shells where the shells are effectively two dimensional (see Figure 1a bottom). To simplify our discussion, we approximate the soft shells as circular disks with radius $r_1/2$ (Figure S13c,d and Figure 1a bottom). In this case, we can approximate the interaction potential between two core-shell particles with separation r as (4)

$$U(r) \approx P_{corona} A_{intersect}(r) \qquad (5)$$

where P_{corona} is the surface pressure exerted by the soft shell for typical polymeric concentrations found in the interacting soft shells and $A_{intersect}(r)$ is the intersection area between the two soft shells at separation r (see Figure S13c,d). From simple geometry, the intersection area is given by

$$A_{intersect}(r) = \frac{r_1^2}{4}(2\theta - \sin 2\theta) \qquad (6)$$

where $\theta = \cos^{-1}\frac{r}{r_1}$. Inserting Eq.(6) into Eq.(5) we finally have

$$U(r) = U_0 \frac{A_{intersect}(r)}{A_{intersect}(r_0)} \qquad (7)$$

which is plotted in Figure 1b for the case of $r_1/r_0 = 4$ (blue curve).

Estimation of U_0 for experimental core-shell system

The height of the repulsive shoulder U_0 can readily be calculated by noting that at the phase boundary between the low density hexagonal phase HEXL and the dimer phase (specifically DIM1, see Figure S6) the enthalpy per particle of both phases are equal, i.e.,

$$U_0/2 + P_{coex} A_{DIM1} = P_{coex} A_{HEXL} \qquad (8)$$

where P_{coex} is the coexistence surface pressure and A_{HEXL} and A_{DIM1} are the area per particle in the low density hexagonal phase and DIM1 phase respectively. The left hand side of eq.(8) is the enthalpy per particle of the chain phase and the $U_0/2$ term comes from the fact that there is one soft shell overlap for every two particles in this phase. The right hand side of eq.(8) represents the enthalpy per particle in

the low density hexagonal phase and there is no energy term as there are no soft shell overlaps in this phase. Rearranging eq.(8) we obtain

$$U_0 = 2P_{coex}(A_{HEXL} - A_{DIM1}) \qquad (9)$$

From Figure S14a, we see that the area per particle for the HEXL phase is $A_{HEXL} = \frac{\sqrt{3}}{2}r_1^2$. From Figure S14b, we see that $\theta_1 = \sin^{-1}(r_0/2r_1)$, $\theta_2 = (\pi - 2\theta_1 - \pi/3)/2 = \pi/3 - \theta_1$, the unit cell angle is $\phi = 2\theta_1 + \theta_2 = \pi/3 + \theta_1$, the unit cell aspect ratio is $\gamma = 2r_1\cos\theta_2/r_1 = 2\cos(\pi/3 - \theta_1)$ and the area per particle for the DIM1 phase is $A_{DIM1} = r_1^2\gamma\sin\phi/2 = r_1^2\cos(\pi/3 - \theta_1)\sin(\pi/3 + \theta_1)$. From Figure 3h, we determine the coexistence pressure to be $P_{coex} \approx 25$ mN/m. Inserting this and $r_1/r_0 = 4$, $r_0 = 170$ nm into Eq.(9), we find $U_0 = 7 \times 10^{-15}$ J, i.e., $U_0/k_BT = 2 \times 10^6$, thus justifying our assumption in the main paper that $U_0 \gg k_BT$.

In order to check that this estimate for U_0 is reasonable, we can also independently calculate U_0 from the work done in compressing two polymeric corona to full overlap which from Eq.(5) is given by

$$U_0 \approx P_{corona}A_{overlap} \qquad (10)$$

where $A_{overlap} = A_{intersect}(r_0) = \frac{r_1^2}{2}\left(\theta_c - \frac{r_0}{r_1}\sin\theta_c\right)$ is the overlap area of two circular disk-like coronas when their corresponding cores are in contact and $\theta_c = \cos^{-1}\left(\frac{r_0}{r_1}\right)$. From the plateau pressure in the surface pressure-area isotherm in Figure 2k, we estimate $P_{corona} \approx 28$ mN/m. Inserting this into Eq.(10) yields $U_0 = 7 \times 10^{-15}$ J, in excellent agreement with our estimate above based on the coexistence pressure. The agreement between the two results confirms that the soft repulsive shoulder in our core-shell particles indeed arises from the elastic compression of the polymer corona around the microspheres.

Comparing our zig-zag chain MEC with that of Fornleitner et al

In this section, we perform a detailed comparison between the zig-zag chain phase found in our minimum energy calculations (i.e., the ZZ phase in Figure 5 or equivalently the ZZ1 phase in Figure S6) and the one found by Fornleitner et al for $r_1/r_0 = 5$ (i.e., Figure 7 of ref.(5)). Specifically, we first calculate the lattice parameters for the ZZ1 phase for a general value of r_1/r_0, use these results to calculate the bond angle and density for $r_1/r_0 = 5$ and compare these with the corresponding values for the Fornleitner et al zig-zag chain phase.

In Figure S15, we sketch a portion of the ZZ1 MEC, where the unit cell is one of the tall red rectangles. From this figure, we see that the unit cell angle $\phi = \pi/2$, the unit call aspect ratio $\gamma = \tan\theta_1$ and the coordinate of the second particle in the lattice basis set is $\alpha = 0.5$, $\beta = 1 - \frac{r_0\sin\theta_2}{r_1\sin\theta_1}$. From the definition of the density parameter ℓ, the area per particle is given by $\frac{\sqrt{3}}{2}\ell^2 = \frac{r_1^2\sin\theta_1\cos\theta_1}{2}$ from which we find $\ell = r_1\left(\frac{\sin 2\theta_1}{2\sqrt{3}}\right)^{1/2}$. In order to find θ_1, θ_2 and hence the lattice parameters as a function of r_1/r_0, we note that from the length of the green line in Figure S15

$$2r_0\cos\theta_2 = r_1\cos\theta_1 \qquad (11)$$

while applying Pythagoras' theorem to the yellow triangle

$$r_1^2 = (r_1\sin\theta_1 - \sin\theta_2)^2 + (3\cos\theta_2)^2. \qquad (12)$$

Solving the simultaneous equations Eqs.(11),(12) yields

$$\cos\theta_1 = \frac{r_0}{r_1}\left(\frac{4r_1^2 - r_0^2}{r_1^2 + 6r_0^2}\right)^{1/2} \qquad (13)$$

$$\cos\theta_2 = \frac{1}{2}\left(\frac{4r_1^2 - r_0^2}{r_1^2 + 6r_0^2}\right)^{1/2}. \qquad (14)$$

Finally, the area fraction is given by $\eta = \frac{\pi r_0^2}{2\sqrt{3}\ell^2}$. On the other hand, referring to Figure S15, the bond vectors $\boldsymbol{u}_1, \boldsymbol{u}_2$ are given by $\boldsymbol{u}_1 = \boldsymbol{b} - (\alpha\boldsymbol{a} + \beta\boldsymbol{b}), \boldsymbol{u}_2 = \boldsymbol{a} + \boldsymbol{b} - (\alpha\boldsymbol{a} + \beta\boldsymbol{b})$ where $\boldsymbol{a} = a(1,0), \boldsymbol{b} =$

$a\gamma(\cos\phi\,,\sin\phi)$ are the lattice vectors and $a = \ell\left(\frac{\sqrt{3}}{\gamma\sin\phi}\right)^{1/2}$ is a lattice constant. The bond angle δ can now be readily found from the dot product of $\boldsymbol{u}_1, \boldsymbol{u}_2$.

Substituting Eqs.(13),(14) into the above expressions and setting $r_1/r_0 = 5$, we find a bond angle of $\delta = 127°$ and an area fraction of $\eta = 0.188$ for ZZ1. In contrast, from an image analysis of Figure 7 of ref.(5) and an analysis of the slope of the Gibbs free energy vs pressure curve in Figure 8 of ref.(5), we estimate a much smaller bond angle of $\delta \approx 68°$ and a much larger area fraction of $\eta \approx 0.70$ for the zig-zag chain phase of Fornleitner et al. These large differences demonstrate that the zig-zag chain phase observed by these authors is not one of our zig-zag chain phases but is instead essentially equivalent to the double chain phase DC in Figure 5 or DC1 phase in Figure S6. There is therefore no contradiction between the results of ref.(5) and our finding that the zig-zag chain phases are only stable for $g \lesssim 2$.

References

1. H. Mehrabian, J. Harting, J. H. Snoeijer, Soft particles at a fluid interface. *Soft Matter* **12**, 1062–1073 (2016).
2. F. Camerin, *et al.*, Microgels Adsorbed at Liquid-Liquid Interfaces: A Joint Numerical and Experimental Study. *ACS Nano* **13**, 4548–4559 (2019).
3. S. Ciarella, *et al.*, Soft Particles at Liquid Interfaces: From Molecular Particle Architecture to Collective Phase Behavior. *Langmuir* **37**, 5364–5375 (2021).
4. M. Rey, A. D. Law, D. M. A. Buzza, N. Vogel, Anisotropic Self-Assembly from Isotropic Colloidal Building Blocks. *J. Am. Chem. Soc.* **139**, 17464–17473 (2017).
5. J. Fornleitner, G. Kahl, Pattern formation in two-dimensional square-shoulder systems. *J. Phys. Condens. Matter* **22** (2010).
6. K. Schwenke, L. Isa, D. L. Cheung, E. Del Gado, Conformations and effective interactions of polymer-coated nanoparticles at liquid interfaces. *Langmuir* **30**, 12578–12586 (2014).
7. F. Camerin, *et al.*, Microgels at Interfaces Behave as 2D Elastic Particles Featuring Reentrant Dynamics. *Phys. Rev. X* **10**, 1–14 (2020).

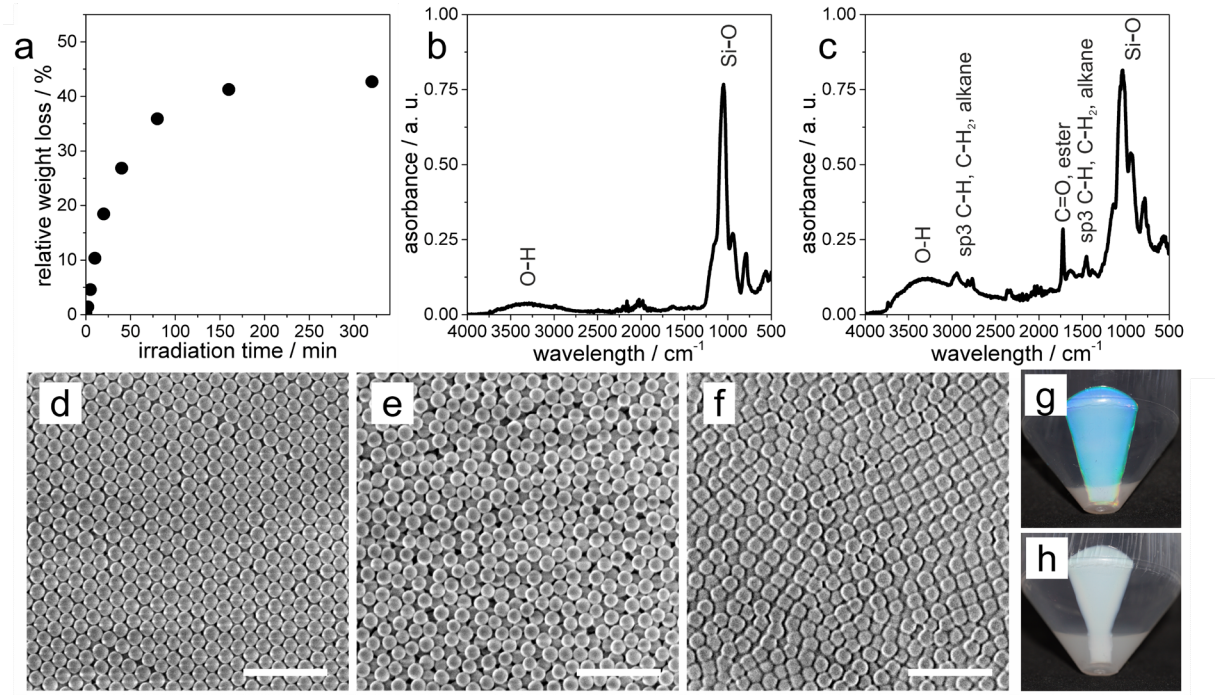

Figure S1. Data for silica particles and shell thickness. a) Thermogravimetric analysis (TGA) data determining the relative weight loss compared to pure silica particles and thus the amount of organic material of core-shell particles at different irradiation times. b) Infrared (IR) spectrum of silica particles c) IR spectrum of SiO_2@PDMAEMA particles at 80 min irradiation time. d) SEM image of dried pure silica particles. e) SEM image of dried iniferter functionalized silica particles. f) SEM image of dried SiO_2@PDMAEMA particles at 320 min of irradiation. g) Photograph of sedimented pure silica particles. h) Photograph of sedimented iniferter functionalized silica particles. Scale bar: 1 µm.

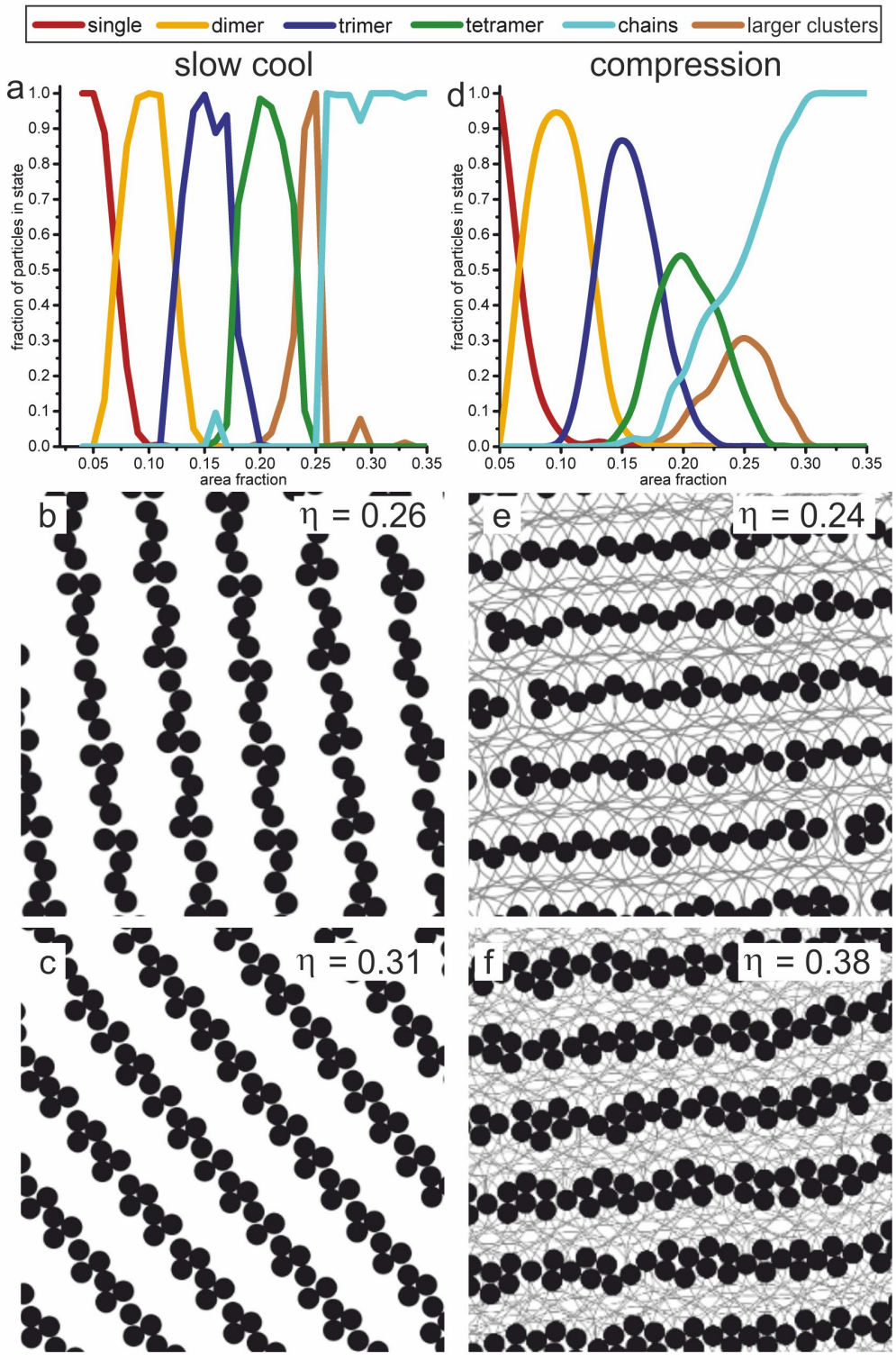

Figure S2. Distribution functions for the different phases and representative complex chain structures obtained from slow cool MC simulations (a-c) and compression MC simulations (d-f) of core shell particles with $r_1/r_0 = 4, g = 1$. Note that both zig-zag chains and braided chains could only be obtained from the compression MC simulations (right snapshots, e,f) but not the slow cool MC simulations (left snapshots, b,c).

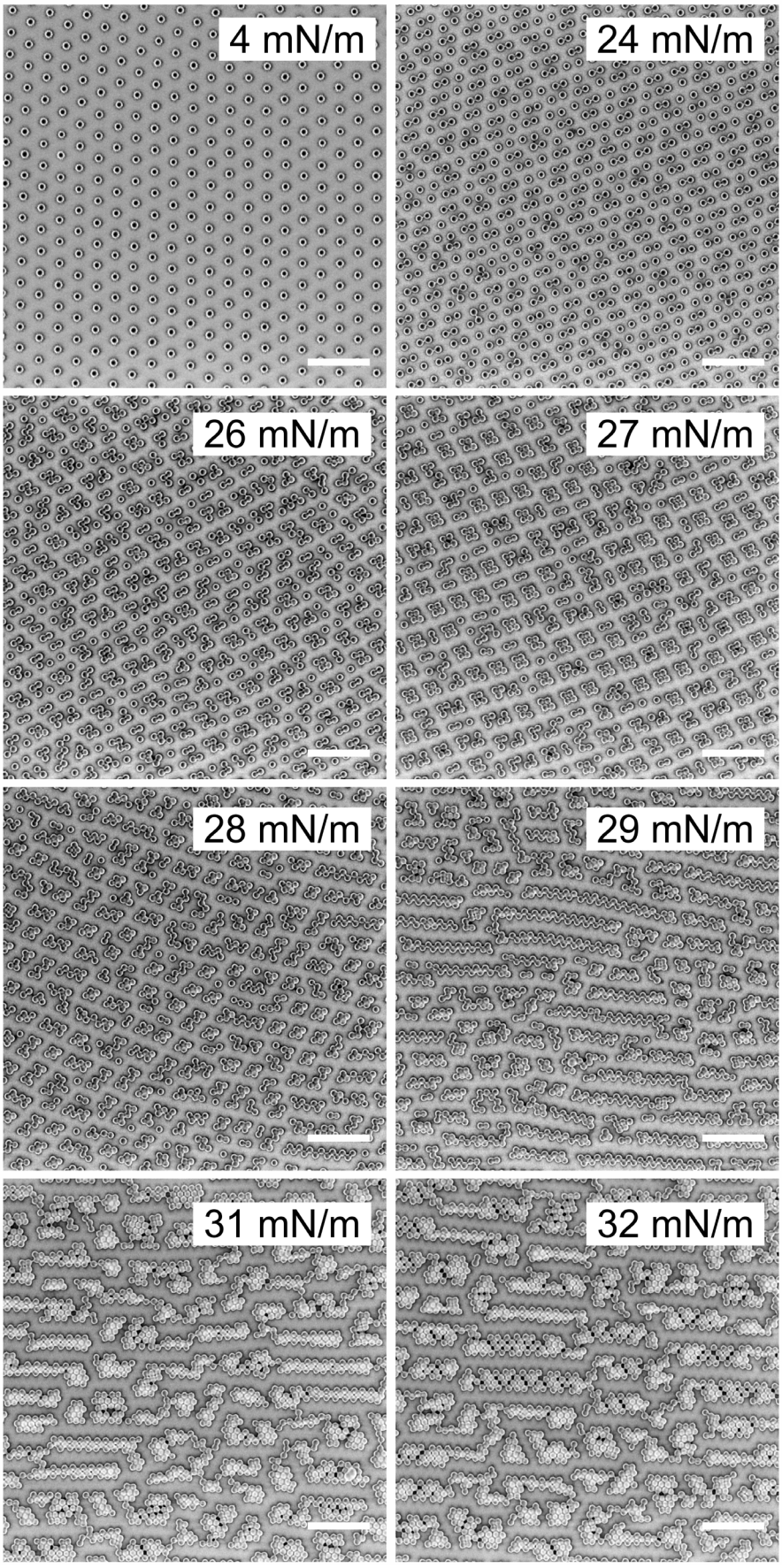

Figure S3. Large area SEM images of the experimental core-shell system with 80 min irradiation at different surface pressures. Scale bar: 2 μm.

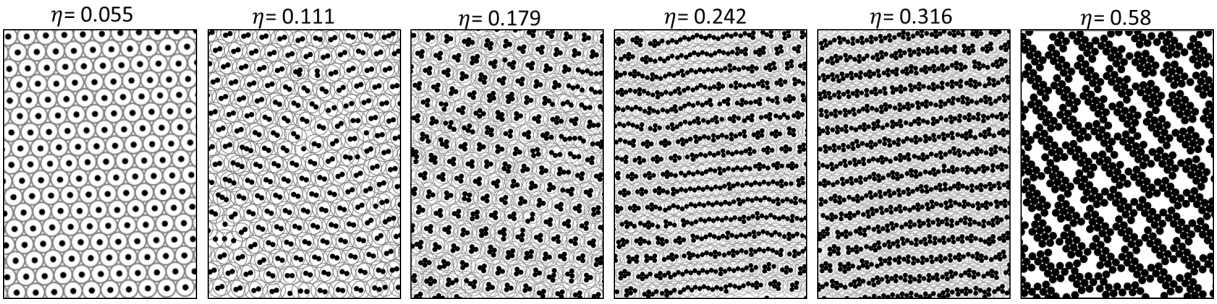

Figure S4. Large area snapshots of different phases obtained from compression Monte Carlo simulations of core-shell particles with $r_1/r_0 = 4, g = 1$. Note that the snapshot for $\eta = 0.58$ was obtained from slow cool MC simulations as the area fraction was too high to be reached using compression MC simulations.

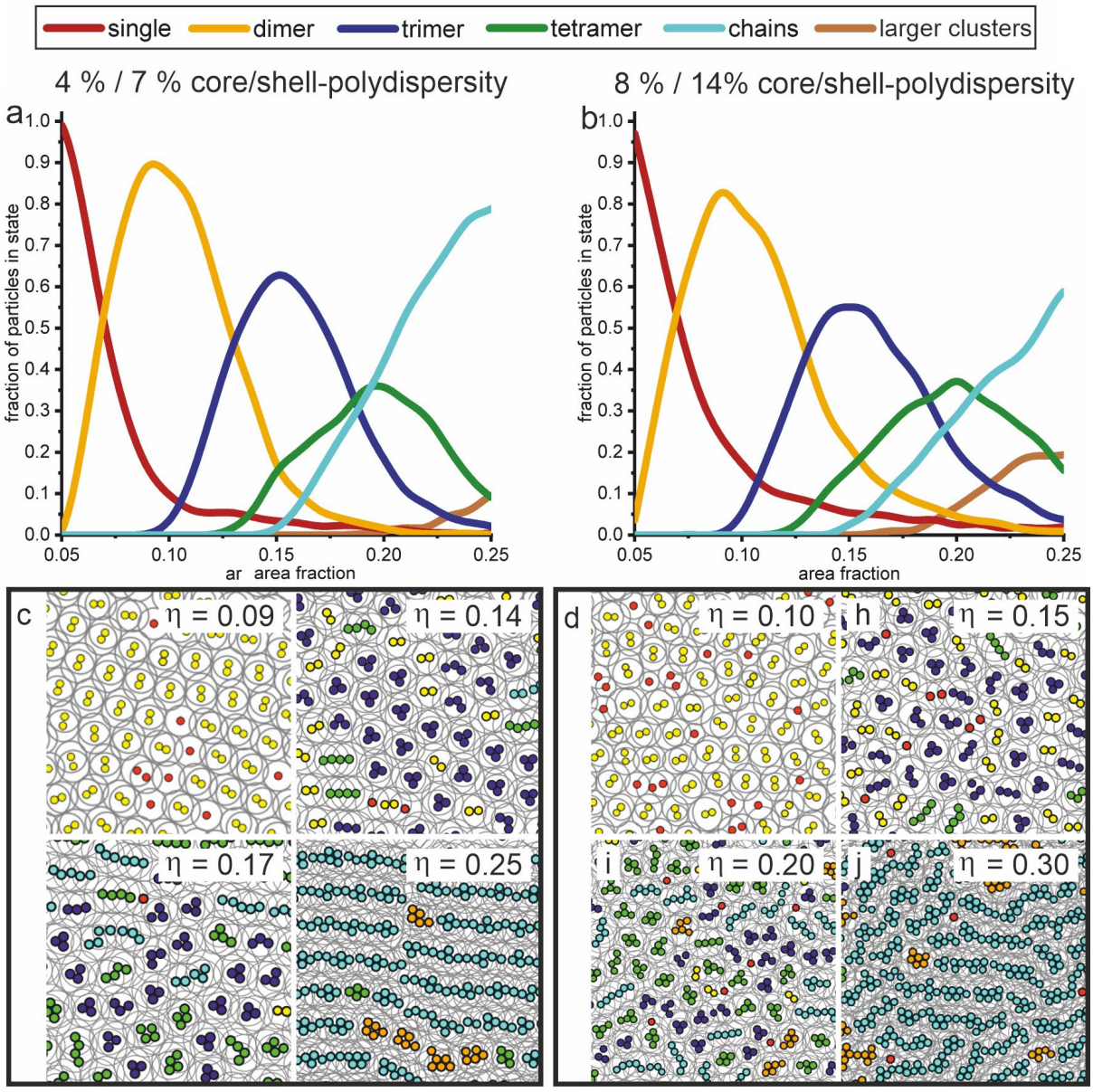

Figure S5. Compression MC simulations of core-shell particles with polydispersity, using $r_1/r_0 = 4, g = 1$, where r_1, r_0 refer to the average shell and core diameter respectively. We assume that the core and shell diameters of the simulated particles follow a Gaussian distribution, with the standard deviation in the core diameter approximately equal to the uncertainty measured by zeta-sizer method and the standard deviation in the shell diameter equal to the uncertainty in the SEM measured nearest-neighbour distance (see Figure 2h) in the data on the left side. On the right, the same simulations are shown with an increased polydispersity of twice the experimental values. a,b) Distribution functions for the populations of the different phases for 4 % core and 7 % shell polydispersity (a) and 8 % core and 14 % shell polydispersity (b); c,d) Snapshots of representative phases for 4 % core and 7 % shell polydispersity (c) and 8 % core and 14 % shell polydispersity (d).

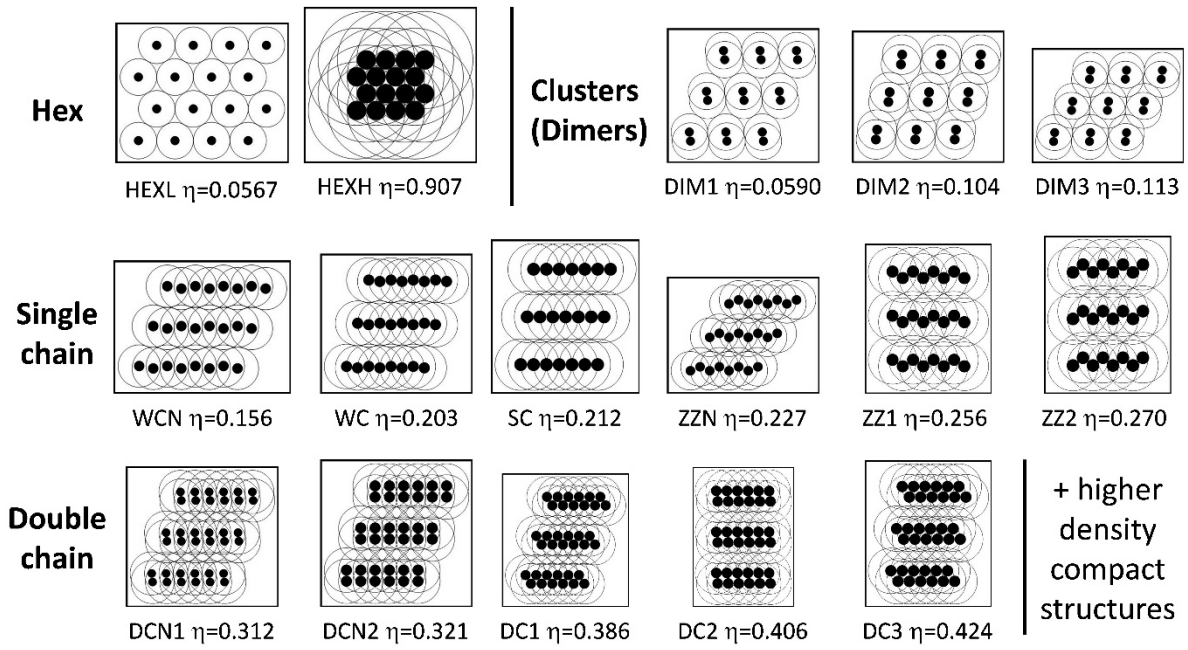

Figure S6. The full set of minimum energy configurations (MECs) containing two particles per unit cell and their corresponding area fractions η for $r_1/r_0 = 4$. In order of increasing η these include: low density hexagonal phase (HEXL), dimers (DIM1, DIM2, DIM3), non-close packed and close packed wavy chains (WCN, WC), straight chains (SC), non-close packed and close packed zig-zag chains (ZZN, ZZ1, ZZ2), non-close packed and close packed double chains (DCN1, DCN2, DC1, DC2, DC3), a series of higher density compact structures, similar to the structures seen at high compression in Figure S4 and finally close-packed hexagonal phase (HEXH). Note that in Figure 5, DIM corresponds to DIM2, ZZ corresponds to ZZ1, DCN corresponds to DCN1 and DC corresponds to DC1.

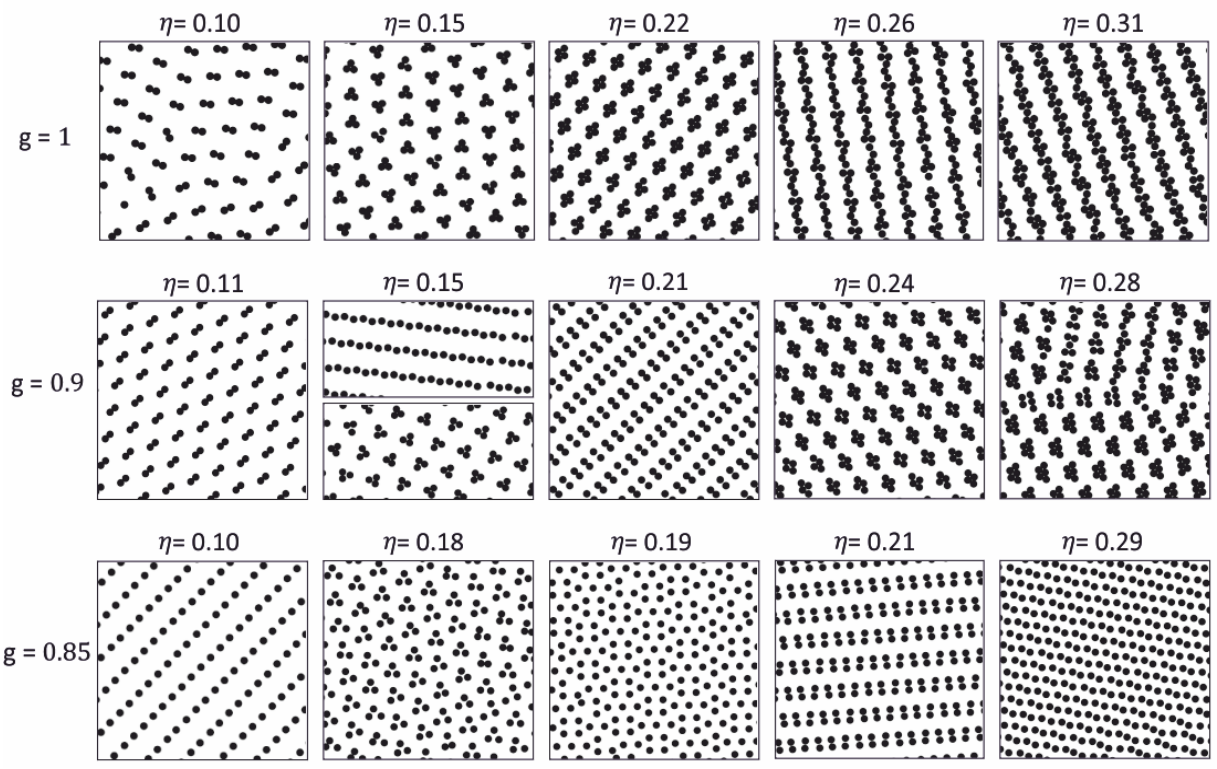

Figure S7. Using Monte Carlo (MC) simulations to bracket the value of g in the experimental systems. Successive rows show the evolution of phases with increasing area fraction η obtained from slow cools MC simulations of core-shell particles with $r_1/r_0 = 4$ and g=0.85; 0.9, 1.0.

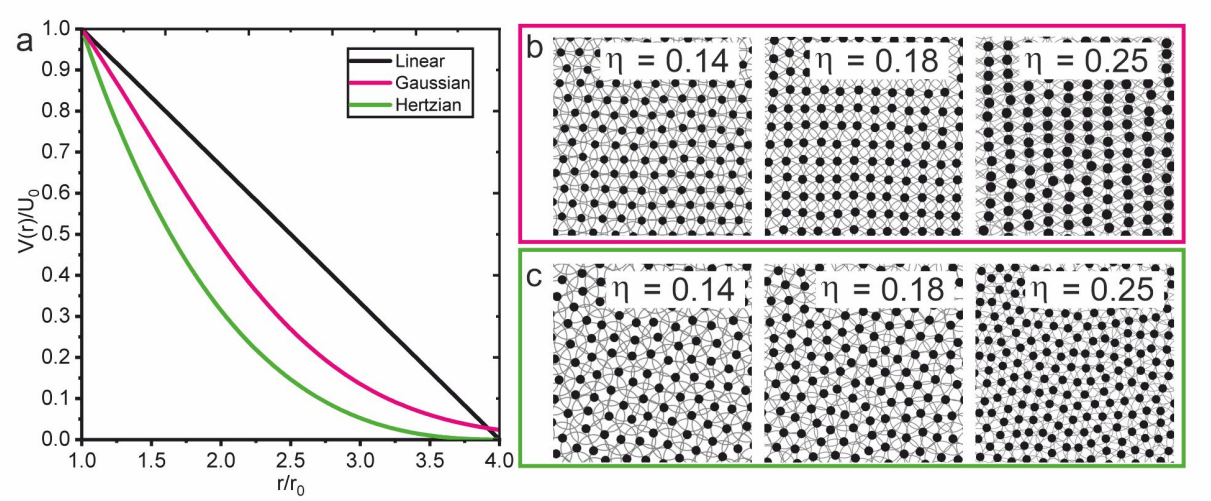

Figure S8. Compression Monte Carlo simulations of core-shell particles interacting via potentials derived from previous monomer-resolved simulations on systems similar to our core-shell particles instead of the linear ramp potential. (a) Plot of the Gaussian potential from ref. (6) given by $V_g(r) = \varepsilon_g e^{-(r/\sigma_g)^2}$ and the Hertzian potential from ref. (7) given by $V_H(r) = \frac{\pi Y \sigma_{eff}^2 (1-r/\sigma_{eff})^2}{2\ln\left(\frac{2}{1-r/\sigma_{eff}}\right)}$ compared to the linear ramp Jagla potential. We choose $\sigma_g = r_1/2$, $\sigma_{eff} = r_1$ and $r_1/r_0 = 4$ so that the range of both potentials is approximately the same as the Jagla potential, and we choose ε_g and Y so that the magnitude of both potentials is U_0 at $r = r_0$. (b,c) Snapshots of characteristic phases for core-shell particles interacting via the Gaussian and Hertzian potentials respectively. None of the characteristic cluster phases are observed for these potentials.

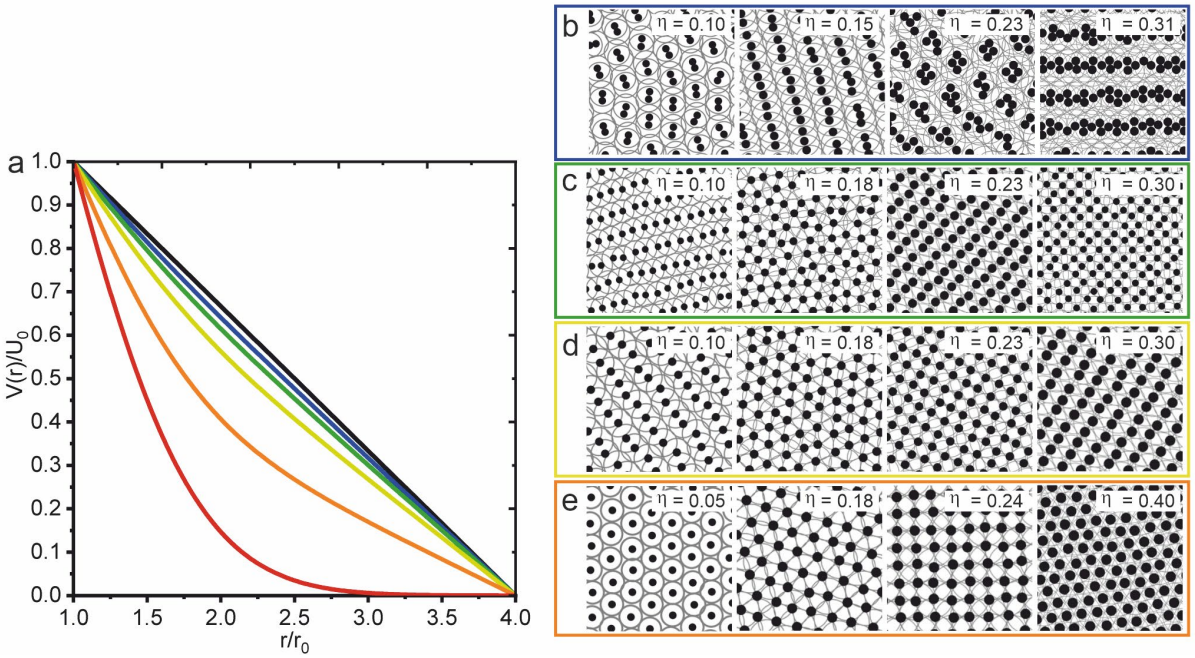

Figure S9. Compression Monte Carlo simulations of core-shell particles interacting via a composite potential consisting of a Gaussian potential and a linear ramp potential with different relative contributions. (a) Plot of the composite potential given by $V(r) = wV_g(r) + (1-w)V_{lin}(r)$ for various values of w, where w is the weighting of the Gaussian potential ($0 \leq w \leq 1$), $V_g(r)$ is the Gaussian potential given the caption for Figure S8 and $V_{lin}(r)$ is the Jagla potential given by Eq.(1) with $g = 1$. Note that following the experimental data in Figure 2h, we choose $\sigma_g/r_0 = 1.25$ and $r_1/r_0 = 4$ so that the range of the linear ramp potential (i.e., due to polymer chains along the interface) is approximately 1.6 times the range of the Gaussian potential (i.e., due to polymer chains swollen into the bulk). (b-e) Snapshots of characteristic phases for core-shell particles interacting via the composite potential with $w = 0.05, 0.1, 0.2, 0.5$ respectively. Cluster and chain phases are only observed for $w = 0.05$.

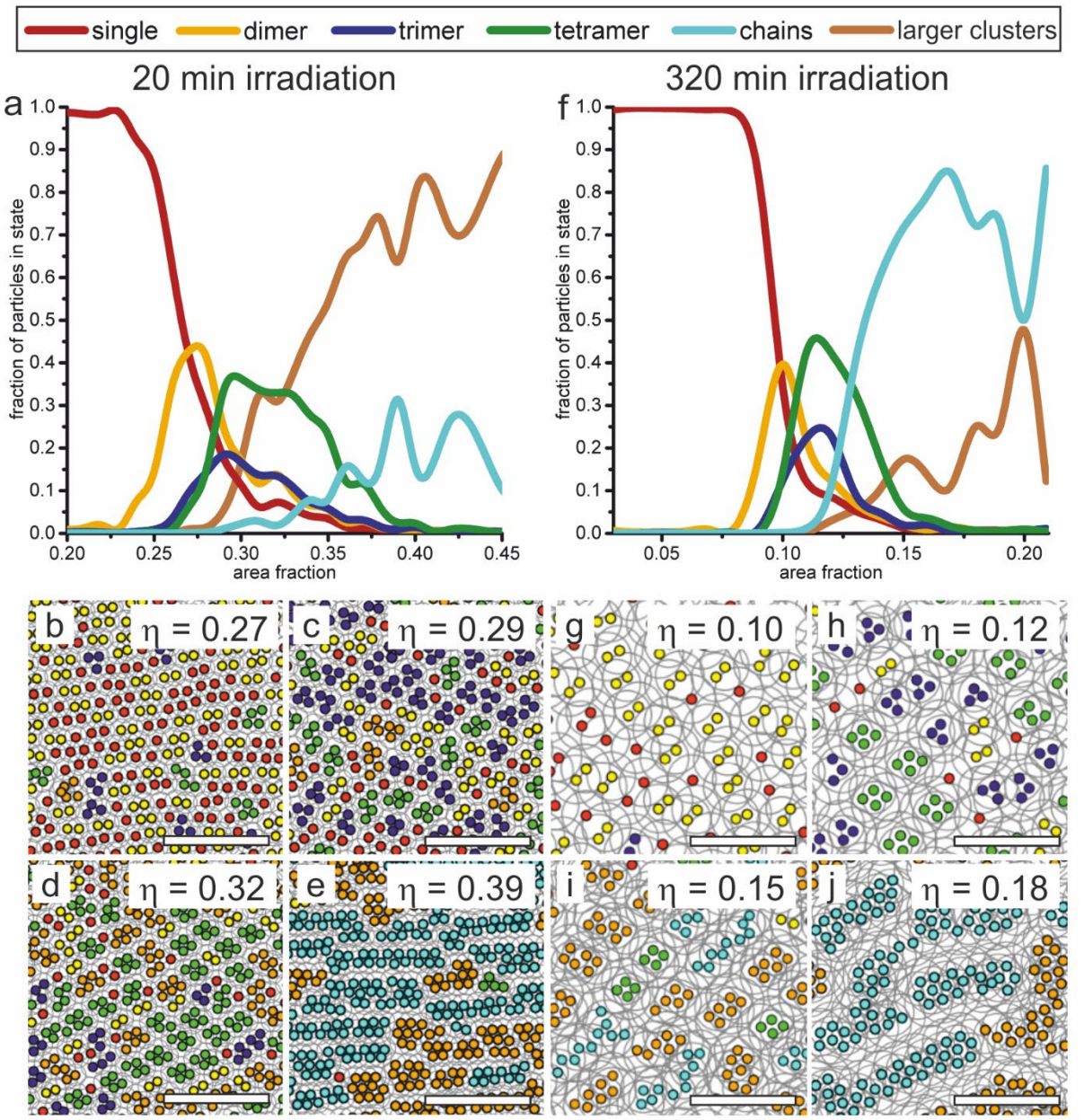

Figure S10: Statistical evaluation of the phase transitions in experiment for 20 min and 320 min irradiation. a) Fraction of particles in different phases as a function of area fraction for 10 min irradiation. b-e) Post-processed SEM images with color-coded cores (d = 170 nm) detected in image analysis for 20 min irradiation. Scale bar: 2µm. f) Fraction of particles in different phases as a function of area fraction for 320 min irradiation. g-j) Post processed SEM images with color-coded cores (d = 170 nm) detected in image analysis for 320 min irradiation. Scale bar: 2µm.

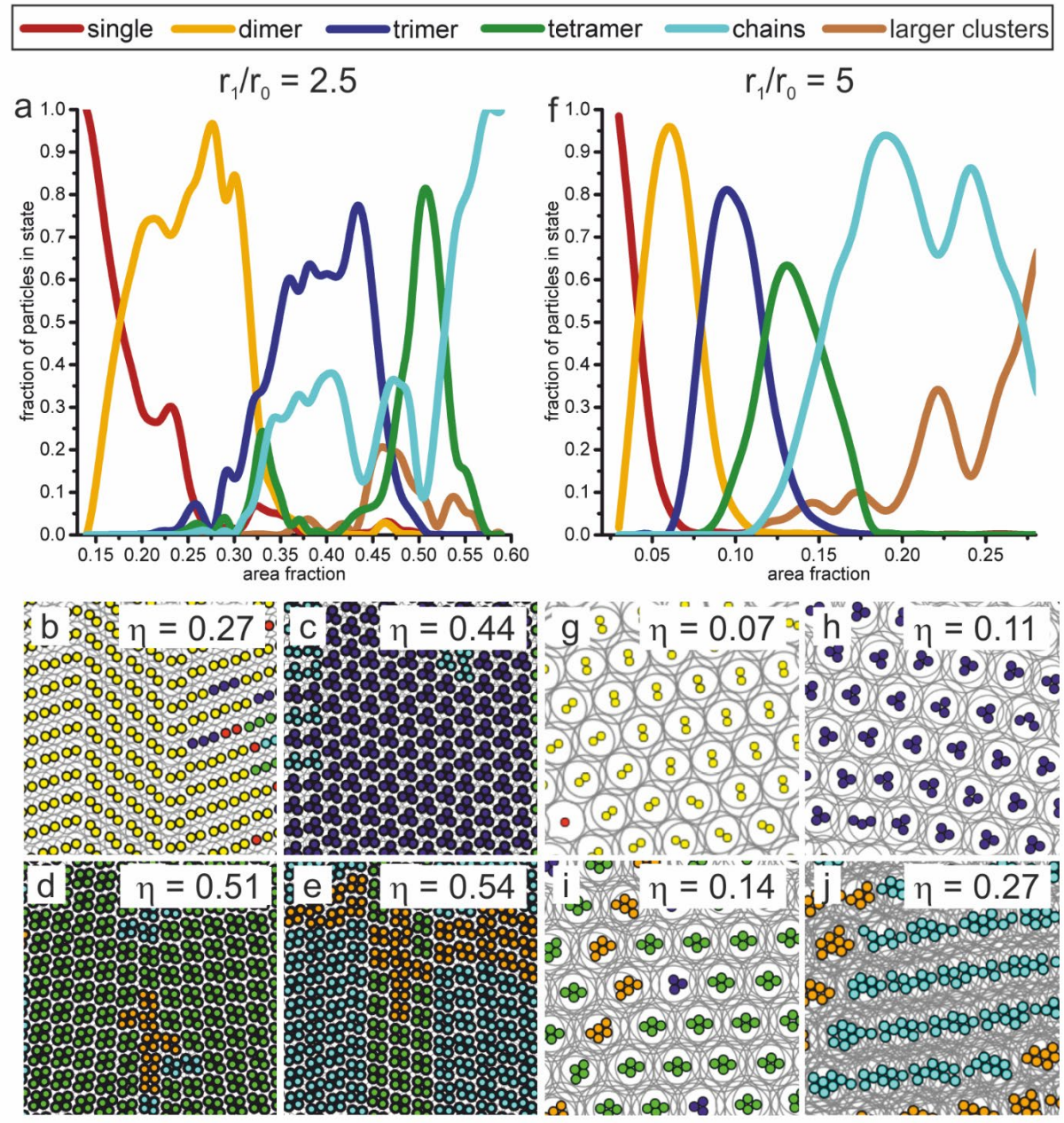

Figure S11. Statistical evaluation of the phase transitions in simulation for r_1/r_0-ratios of 2 and 5. a) Fraction of particles in different phases as a function of area fraction for r_1/r_0 = 2.5. b-e) Simulation snapshots with color-coded phases detected in image analysis for r_1/r_0 = 2.5. f) Fraction of particles in different phases as a function of area fraction for r_1/r_0 = 5. g-j) Simulation snapshots with color-coded phases detected in image analysis for r_1/r_0 = 5.

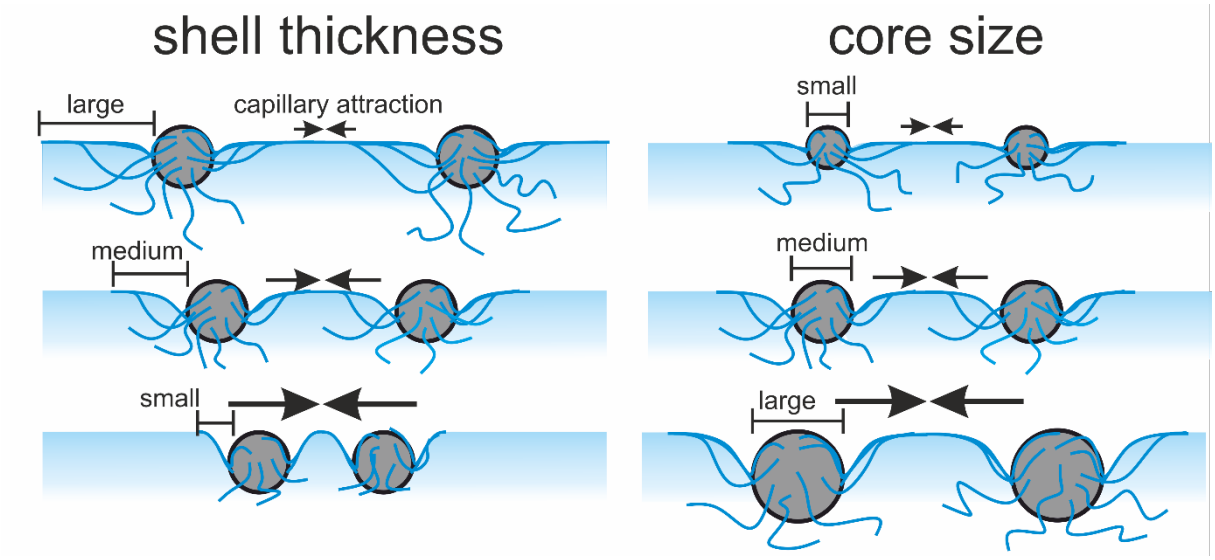

Figure S12. Schematic illustration of the effect of attractive capillary forces that can cause aggregation for small shell dimensions or larger core particles. The best agreement of the experimental phase behaviour with the theoretical Jagla phases is observed if capillary forces are suppressed, either by large shell thicknesses or small core sizes.

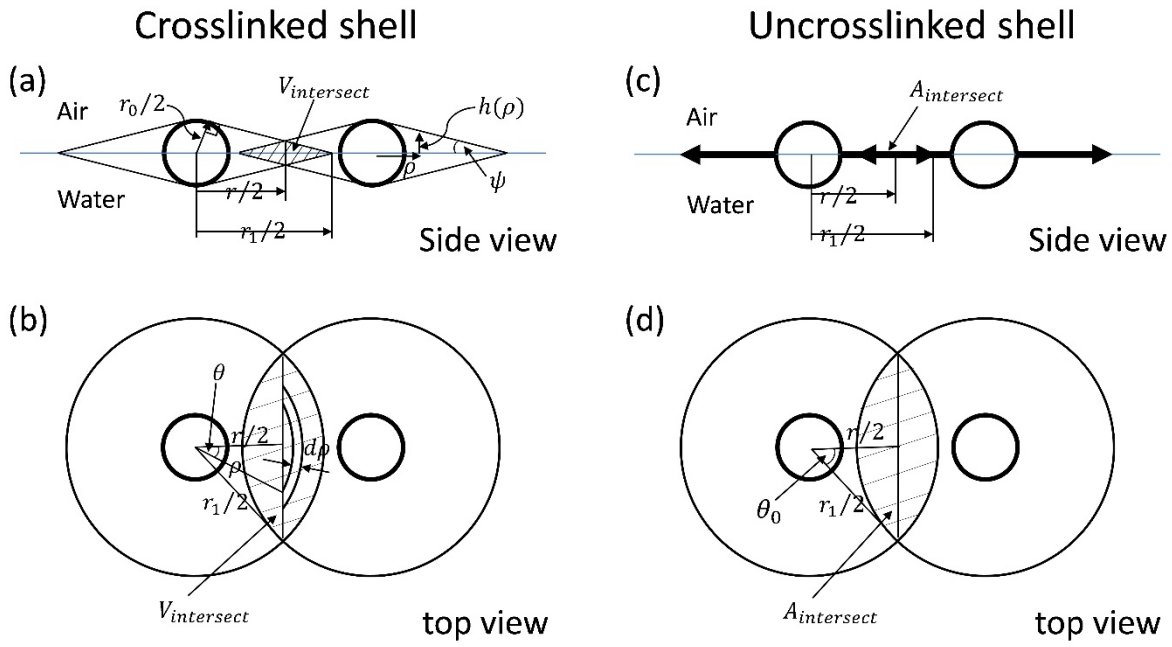

Figure S13. Simplified geometry used to calculate the soft shell repulsion for crosslinked shells (a,b) and uncrosslinked shells (c,d). The thick and thin circles represent the core and shell respectively. A 3D view of both cases is shown in Figure 1a.

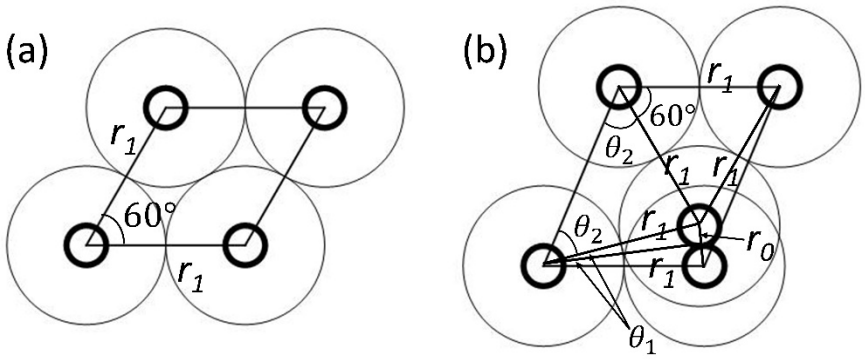

Figure S14. Unit cell and geometrical parameters for (a) HEXL phase; (b) DIM1 phase. The thick and thin circles represent the core and shell respectively.

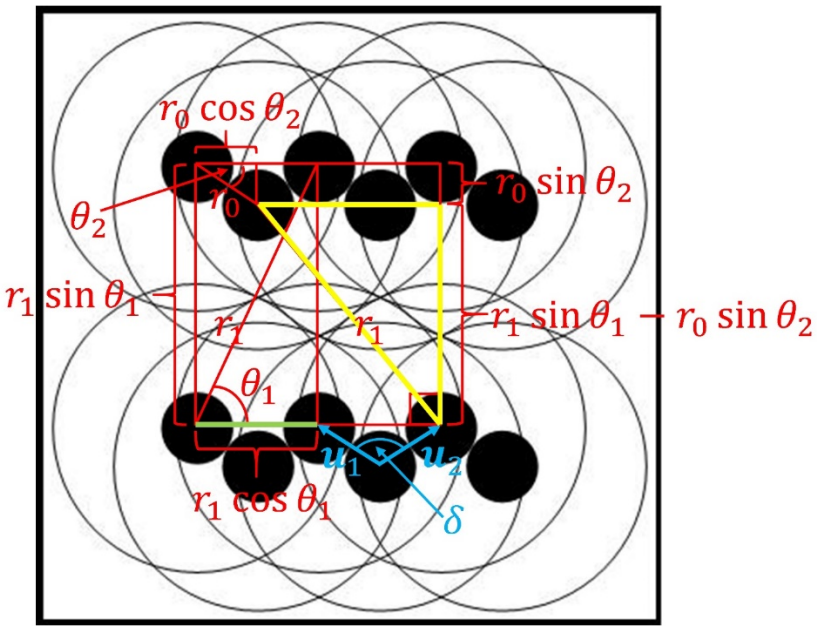

Figure S15 Geometric parameters for the ZZ1 phase. The solid disks and thin circles represent the core and shell respectively.

Movie S1: Animated Monte-Carlo compression simulation for particles with $r_1/r_0 = 4$. Legend, area fraction and scale are visible in the movie.

Movie S2: Animated post-processed SEM-images for particles with an irradiation time of 80 min. Legend, area fraction and scale are visible in the movie.